ACS APPLIED MATERIALS & INTERFACES

Research Article

www.acsami.org

Multiple Step Growth of Single Crystalline Rutile Nanorods with the Assistance of Self-Assembled Monolayer for Dye Sensitized Solar Cells

Mengjin Yang, Suman Neupane, Xuewen Wang, Jin He, and Wenzhi Li*

Department of Physics, Florida International University, Miami, Florida 33199, United States

Nezih Pala

Electrical & Computer Engineering, Florida International University, Miami, Florida 33174, United States

Supporting Information

ABSTRACT: A novel multiple step growth (MSG) process has been developed to synthesize rutile nanorods (NRs) on fluorine-doped tin oxide (FTO) glass with the assistance of a self-assembled monolayer (SAM) aiming to increase the internal surface area of the 1D materials for dye sensitized solar cell (DSSC) applications. The experimental result reveals that the SAM layer can be selectively decomposed at the tip of the nanorod, namely the rutile (001) surface, due to the anisotropic photocatalytic property of the rutile. The remaining SAM layer on the side-wall of the NRs remains intact and serves as water repellent which prevents the radial growth of the NRs during the next step hydrothermal synthesis; therefore, the spacing between the NRs and the porosity of the NR array can be retained after additional growth cycles. On the other hand, introduction of a middle layer formed via $TiCl_4$ solution treatment before the next growth cycle is found to be an effective way to control the diameters of the newly grown NRs. The performance of DSSC made from the rutile NRs grown using the MSG technique has been examined, and it is significantly affected by the internal surfaces of the NRs. Furthermore, the MSG combined with NR etching treatment by acid at low temperature (150 °C) leads to a significant enhancement in the solar cell performance. The gigantic wettability difference of the NRs before and after the SAM treatment as well as the MSG method could be adapted to prepare superhydrophobic and superhydrophilic nanostructured patterns for other applications.

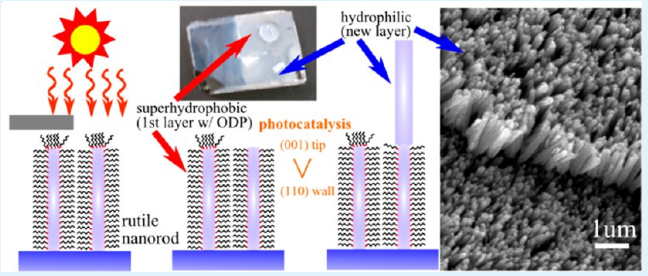

KEYWORDS: *rutile nanorod, multiple step growth, self-assembled monolayer, superhydrophobic, superhydrophilic, dye sensitized solar cell*

INTRODUCTION

One dimensional (1D) structure, especially vertically aligned nanowire/nanorod on top of a substrate, has been proposed as an alternative photoanode in dye sensitized solar cells (DSSCs) to reduce numerous trapping sites in the conventional particulate architecture.[1−8] Although anatase is preferred over rutile in DSSCs in terms of electron transport, rutile nanorods is still very popular due to its single crystal structure and facile fabrication. A more rapid charge transport in nanorod (NR) based device was reported comparing with those made of rutile nanoparticles.[9,10] Surface area is one crucial problem for NRs since it determines the dye loading, and, consequently, the absorption of incoming light. Several approaches have been conducted to address this low surface area issue. One approach is the adaption of a thin absorber with a large absorption coefficient, such as perovskite sensitizer, to capture most of light in a submicrometer length.[11] Another approach is to increase surface area of nanorods, for example, by introducing hierarchical structures such as branched structure[12,13] or by simply growing long nanorods through multiple cycle growth and alternative precursor recipes. Multiple cycle growth of NRs with the addition of saturated sodium chloride solution has been conducted by Zhou et al., but the losses of internal surface area, transmittance, and bonding degraded the performance of the long NRs.[14] Synergetic interaction between $TiCl_4$ and octanoic acid has been adapted to achieve long NRs with high surface area, but the NRs form bundles with each other as the reaction time goes after 12 h resulting in a decrease in specific surface area of the NRs.[15] In contrary, acid etching of pregrown NRs has been found to be an effective way to break the bundles of the NRs, and significant increase in energy conversion efficiency has been reported.[16,17] However, the NRs used for the etching experiment has not been grown more than 8 μm, which is much shorter than the estimated optimal length (20

Received: July 24, 2013
Accepted: September 13, 2013
Published: September 13, 2013

   dx.doi.org/10.1021/am4030092 | ACS Appl. Mater. Interfaces 2013, 5, 9809−9815

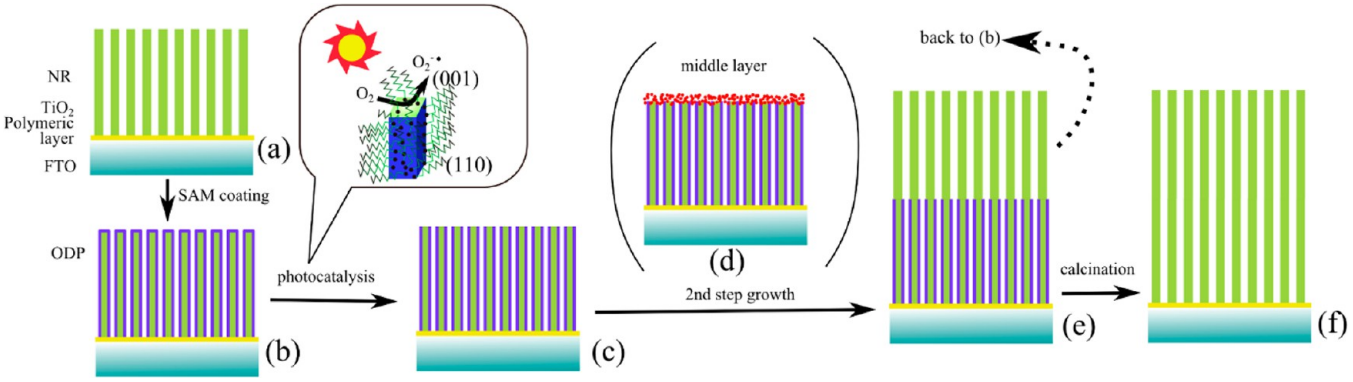

Figure 1. Schematics of multiple step growth of NR with the ODP protection. (a) As-grown NRs, (b) SAM coated NR, (c) NRs with tips opened via anisotropic photocatalysis, (d) adding of a middle layer using $TiCl_4$ treatment, (e) second step growth, (f) removal of the remaining SAM by calcination. Dashed lines show optional growth routes: second step growth without a middle layer and multiple growth cycles.

μm).[10] Recent development of etching has achieved long nanorods by using high $TiCl_4$ loading, but the NRs are easily detached from the first layer in the second step procedure due to the preferential interface etching.[18]

Surface area of NR has been increased in many ways, but there is still a long way to make a breakthrough in NR based solar cells. After post-treatments, surface area may not be high enough some times, and/or the increased surface area is constrained by other charge transport factors. Several side effects have been reported after treatments, such as increased electron recombination,[18,19] reduced transport time,[9,19] and poor adhesion to fluorine-doped tin oxide (FTO).[15] Despite the aforementioned efforts, the NR based DSSC is still falling behind nanoparticle based device in terms of efficiency because it is difficult to increase the length of the NR array without sacrificing the porosity and a good charge transport. Herein we report a multiple step growth approach via the assistance of self-assembled monolayer (SAM) to solve the issue of porosity decrease. It has been reported the successful multiple step growth of ZnO nanowire with SAM layer protection.[20] The beauty of the SAM protection approach is that the internal surface of an existing layer of NRs is not affected while a new layer of NRs is growing on top of the existing layer, and as a result, the overall surface area of the multiple-step grown NRs will be increased substantially. Although the SAM protection approach is a promising progress, it is very challenging to apply to the synthesis of single crystalline rutile NRs. First of all, the reaction environment in rutile NRs synthesis is much harsher (with a high hydrochloric acid concentration at a relatively high temperature varying from 150 to 200 °C) comparing to the mild ZnO nanowire growth condition. Second, the ZnO nanowire used in the reported paper is fairly large in width (around 200 nm) and thick in length (10 μm), which provides a good chance of removing top SAM cap layer using ultraviolet ozone, while rutile NRs possess subhundred nanometer width and only a few micrometers thickness. We have managed to overcome the aforementioned barriers by carefully selecting SAM material and utilizing the unique anisotropic photocatalysis of rutile crystal.

The SAM we have chosen is octadecylphosphonic acid (ODP, $CH_3(CH_2)_{17}PO_3H_2$) which has a strong hydrolytic stability especially in acid condition[21] as well as temperature stability in air.[22] The ODP layer is uniformly coated around each NR. Opening the tip of the NRs coated with ODP layer is realized by decomposing the ODP layer at the tip of the NRs by utilizing the photocatalytic property of TiO_2. Decomposition of ODP on rough anatase film[23] and nanotube[24] has been reported using TiO_2 photocatalysis, and moreover anisotropic photocatalytic property has been observed.[25,26] It is found that rutile (001) shows higher photocatalytic activity than rutile (110) and (100).[27] Rutile NR grown on FTO substrate has a well-defined crystal structure: (110) is the NR's side wall and (001) is the NR's top surface.[5] Since the (001) face has a higher photocatalytic activity, it is reasonable to expect that the SAM layer on the (001) face will be removed first if the sample is exposed to light. Then, the tip-opened NRs can be put back in the hydrothermal synthesis for the next step growth. Indeed we achieved rutile NRs with increased length after multiple step growth (MSG) with the assistance of ODP. The NRs show a considerable increase of their internal surface area. The new paradigm may pave a way to achieve high efficient nanorod-based dye sensitized solar cells.

EXPERIMENTAL SECTION

Nanorod Growth. Fluorine-doped tin oxide (FTO, Pilkington TEC 7) was modified with a TiO_2 polymeric sol as described previously.[9] Regular nanorod growth as well as nanorod growth with HCl etching can be found in detail at the Supporting Information.

The obtained NRs went through a series of procedures as depicted in Figure 1 to finish a multiple step growth. The ODP SAM surface treatment was conducted in the way similar to the reported method[28] with some modifications. Briefly, 1 mg of ODP (Alfa Aesar) was dissolved into a solution consisting of 10 mL *n*-heptane (Alfa Aesar) and 70 μL isopropyl alcohol (IPA). A piece of FTO substrate with NRs was immersed into the prepared solution for overnight to obtain a good SAM layer coated on the NRs as shown in Figure 1b. Then, the SAM-modified NRs were exposed to a solar simulator for a certain time so that the tips of the NRs were opened by the photocatalysis of TiO_2 under the light irradiation. The tip-opened NRs proceeded to have directly a second hydrothermal growth as seen from Figure 1c–e, and some samples were added a porous middle layer using $TiCl_4$ treatment prior to the second step growth as shown in Figure 1d. The middle layer was formed by bathing the NRs in a 8 mM $TiCl_4$ aqueous solution at 50 °C for 1 h and followed 120 °C baking for 30 min. NRs can grow multiple times to increase their length by simply repeating the procedure as shown in Figure 1b–e. Finally, the remaining ODP on the walls of NRs was cleaned by calcination in air at 500 °C for 2 h to obtain clean NR arrays, as shown in the Figure 1f. In order to avoid the calcination effect, control samples without MSG have the same calcination process as NR treated with ODP.

DSSC Device Assembly. Photoanode of NRs grown on FTO from the above method was immersed in a 0.3 mM ditetrabutylammonium *cis*-bis(isothiocyanota)bis(2,2′-bipyridyl-4,4′-dicarboxyla-

to) ruthenium(II) (commonly known N719, Sigma-Aldrich) ethanol solution overnight for a complete dye adsorption. The counter-electrode was prepared as follows: a drop of 5 mM H_2PtCl_6 in IPA solution was put on a clean FTO substrate and dried in air, and then, the FTO was further heated at 400 °C for 10 min to obtain Pt through a thermal decomposition. A 60 μm hot-melt sealant Surlyn (Meltonix 1170, Solaronix) film was used as a spacer to form a sandwiched structure of photoanode, electrolyte, and counterelectrode. The composition of the electrolyte is 0.6 M 1-butyl-3-methyl-imidazolium iodide (BMII, Sigma-Aldrich), 0.03 M iodide (Sigma-Aldrich), 0.1 M guanidinium thiocyanate (GSCN, Sigma-Aldrich), and 0.5 M 4-tertbutylpyridine (TBP, Sigma-Aldrich) in 85 v/15 v acetonitrile/valeronitrile solution. The electrolyte was filled in between the two electrodes through a predrilled hole on the counterelectrode using a vacuum-backfilling technique. The hole is sealed by a glass slide after the electrolyte filling. External electrodes were painted with silver paint for good contact.

Characterization. The morphology of the NRs was observed via a field-emission scanning electron microscope (JEOL JSM 6335F) and transmission electron microscope (FEI Tecnai F30). Structure of the NRs was characterized by X-ray diffractometer (Siemens D5000) with a Cu Kα1 source. The internal surface area of the NR array was estimated through a dye desorption measurement.[29] Briefly, sensitized photoanode was immersed into a 2 mL 0.2 M NaOH in ethanol/DI solution for 2 h to completely desorb the dye. The dye concentration was calculated from its absorption spectrum which was obtained from a UV/vis spectrometer (Ocean Optics USB2000). Current−voltage (I−V) measurement on the solar cells was carried out using a sourcemeter (Keithley 2400) under AM 1.5 condition from Xeon arc lamp (New Port), which was calibrated by a standard silicon reference cell. Electrochemical impedance spectroscopy was measured at 5 mV alternating voltage from 0.1 Hz to 100 kHz with a negative 0.8 V bias under 1 sun condition using a potentiostat (CHI 760D).

RESULTS AND DISCUSSION

Synthesized nanorod has a width from 15−30 nm (single nanorod) to 40−60 nm (bundles) as shown in the low magnification transmission electron microscopy (TEM) image in Figure 2a. Figure 2b gives a high resolution TEM image of a single nanorod in rutile phase, which presents the (110) planes parallel to the growth direction of the nanorod. Selected area diffraction patterns (Figure 2c and d) at different zone axes ZA [1$\bar{3}$1] and ZA [1$\bar{1}$1] show that the NRs have a single crystalline rutile phase and grow in the direction of ⟨001⟩ (⟨310⟩ × ⟨110⟩ = ⟨001⟩). The X-ray diffraction (XRD) pattern in Figure 2e also proves that NRs are in rutile phase. The stronger (002) peak indicates the vertical growth of NRs on FTO substrates. Such a well-oriented single crystal provides the foundation for the anisotropic photocatalysis.

The first question we need to address is whether the ODP SAM layer works in the NR growth condition. Since there is a dramatic change of water wettability on NRs before and after the ODP modification as shown in Supporting Information Figure S1, a good indicator of the opening of the top layer of ODP coating is the contact angle (CA) between a water droplet and the surface of the NR array. The as-grown NRs present a superhydrophilicity because of the porous structure and hydrophilic surface of the TiO_2 NRs. However, the CA goes to a very high value after the ODP modification indicating a superhydrophobicity. The superhydrophobicity comes from densely aligned carbon chains of ODP on the surface of the NRs. When the NRs are exposed to a simulated solar light the CA decreases with the increase of the exposure time indicating the progressive decomposition of the ODP layer. The removal of the ODP layer will be more profound at the top surfaces of the NRs due to the strong photocatalytic effect of the (001)

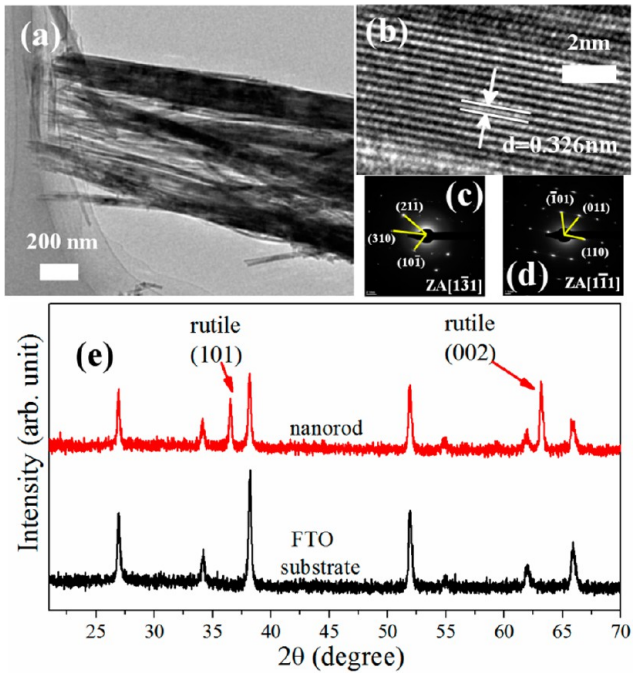

Figure 2. TEM micrographs of nanorods at low magnification (a) and high resolution (b), selected area diffraction pattern at zone axis [1$\bar{3}$1] (c) and [1$\bar{1}$1] (d), and XRD pattern of nanorod array on top of FTO substrate (e).

surfaces of the NRs. To further demonstrate the selective photocatalytic removal of the ODP coating and the survivability of the ODP under the hash NR synthesis condition, a sample of NR array grown on FTO substrate was coated with ODP, and then, a mask was used to block light for half of the NR array during the photocatalysis process. As a result, the masked half sample was covered by ODP layer and the other half was opened at the top. This sample was then put into an autoclave for a second step growth of the NRs. Figure 3a presents a photo

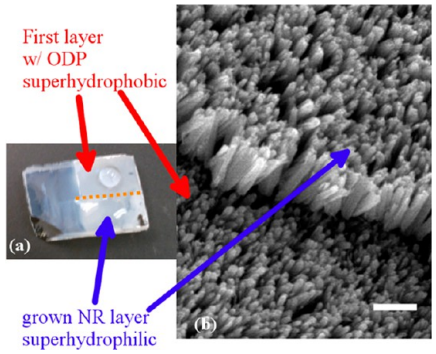

Figure 3. Photo showing the wettability (a) and a tilted-SEM view (b) of the half-masked NRs after the second hydrothermal growth, scale bar in part b is 1 μm. A dotted line in part a indicates the border of the first superhydrophobic layer with ODP and the second super-hydrophilic layer.

of the half-masked sample after the second step growth and the wettability test. There were two distinct regimes on the surface of this sample: one region is superhydrophilic while the other is superhydrophobic. As mentioned above, superhydrophobicity is due to the well-covered ODP layer, and its existence indicates that ODP coated SAM layer withstands the hydrothermal

reaction condition. The superhydrophilic part is the freshly grown second layer of NR array, which is verified by the SEM observation as shown in Figure 3b. Results from the half-masked NR array clearly demonstrate the success of growing a second layer of NRs with the ODP assistance. In addition, the high contrast of wettability using one mask could find its niche in other applications, such as fabrication of superhydrophilic/superhydrophobic patterns.[30]

The change of CA reflects how well the ODP layer anchors to the surface of the NRs. The decrease of CA indicates the removal of the ODP layer by the photocatalysis. On the basis of our selective decomposition experience, CA below 50° is a good indication of removal of the top ODP layer. Cyclic voltammetry results of pure NRs, ODP coated NRs, and ODP coated NRs after tip opening, which can be found in Supporting Information Figure S2, illustrate the successful coating and opening of the ODP layer. The light source we used is a simulated solar light instead of pure UV light. UV light will be more efficient in terms of photocatalysis because of the wide band gap nature of the rutile (~3.0 eV). ODP coated NRs with a UV light treatment easily turn to be superhydrophilic, but it is also observed that the CA increases when the UV irradiated sample was kept in dark for a few hours. The superhydrophilicity of the UV irradiated TiO_2 comes from the change of surface states of TiO_2 with more Ti^{3+} sites, which is favorable for the adsorption of hydroxyl groups due to its corresponding oxygen vacancy.[31] If the UV irradiated sample is left in dark ambient, the adsorbed hydroxyl group is replaced by oxygen in air, and the wettability of the TiO_2 returns to be hydrophobic.[32,33] The superhydrophilicity resulted from the absorbed hydroxyl group may not indicate a complete opening of the NR tip, and the second growth of the NRs may not succeed. On the other hand, simulated solar light contains both UV and visible light, and it gives a relatively slow but steady removal of the ODP layer. It has been reported that the visible light can help to get rid of the adsorbed hydroxyl group due to the accompanied heat and cause CA to increase.[34] The combination of UV and visible light in the simulated solar light results in a smooth change of wettability of ODP coated NRs.

Figure 3 shows that the NRs from the second step growth are different from the NRs from the first step growth. NRs from the second step growth have larger width and reduced density compared with those from the first step growth. For a single layer of NRs, only a fraction of NRs could manage to reach the top due to the nonideal vertical growth;[5,35] therefore, the density at the top is usually reduced compared with the density at the bottom. In addition, the size of the NR tip in the first layer is much larger compared with polymeric seeding layer.[9] The number and size of the seeding sites on top of the first layer of NRs likely have contributed to the thicker NRs during the second step growth. To circumvent this issue, a middle layer of TiO_2 particles is introduced prior to the second growth as shown in Figure 1d. Figure 4 shows the morphology of the NRs after the second step growth without (Figure 4a) and with (Figure 4b) the use of the middle layer. Without the middle layer, the top layer NRs are much thicker with a size of more than a hundred nanometers, as shown in Figure 4a. The inset in Figure 4a presents the interface between the two layers of the NRs. It can be seen that the bottom of the NRs from the second step growth is tapered to accommodate the size differences between the two lays. On the other hand, if a TiO_2 middle layer is used, the width of the NRs from the second step growth does not increase significantly comparing with the

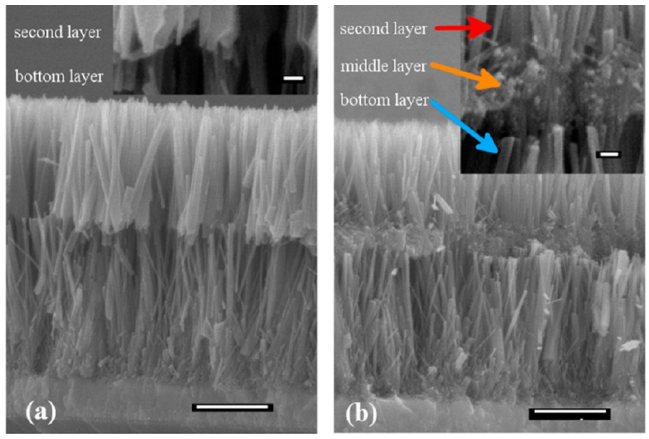

Figure 4. SEM cross-section view of the second step growth of NR without (a) and with middle layer (b). The insets show the interface between the two layers. Scale bars are 1 μm for main figures and 100 nm for insets.

width of the NRs from the first step growth. The NRs from the first and second step growth have a width in the similar range of 40−60 nm (see Figure 4b and its inset). The middle layer of TiO_2 is formed via a 60 min $TiCl_4$ solution treatment and is around 300 nm thick from Figure 4b inset, and this middle layer is suitable as the seeding layer for the second step growth. It is worth pointing out that the NRs from the multiple step growth using middle layer are porous enough to allow dye adsorption and electrolyte infiltration.

A series of multiple-step grown NRs with a middle layer have been prepared at 180 °C for the first step growth and at 170 °C for the following step growth for 5 h, and the samples grown from first step, second steps, and third steps are named as 1S, 2S, and 3S, respectively. The average lengths of the 1S, 2S, and 3S NRs are 2.7, 3.9, and 5.1 μm, respectively, as shown in Figure 5. It is evident that the ODP SAM layer plays an active role in retaining the morphology of the prior NRs after the additional growth cycles. Although SAM layer seems to be weak, it is strong enough to repel the harsh reaction solvent and successfully protect the bottom layer of NRs from further reaction. The growth rate of the NRs is repeatable and stable for the multiple step growth. The length of the NRs from the second and third step growth is shorter than that of the NRs from the first step growth. The shorter length of NRs from the second and third growth can be attributed to the lower growth temperature (170 °C) comparing with that of growth temperature (180 °C) for the first step growth.[9] In the multiple step grown NR sample, the later NR layers have higher density than the prior ones due to use of the middle layer, as shown in Supporting Information Figure S3. These results indicate that the internal surface area of the NR array after the multiple step growth can be significantly increased by extending the length and increasing the density of the NRs.

The middle layer serves as a fresh starting point in multiple step growth, and theoretically, it can be applied as many times as possible to grow the NRs to a desired length while the NRs from prior growth steps still keep their original width which is realized by utilizing the ODP SAM. It needs to be pointed out that the back side of the FTO glass will be severely damaged after several growth cycles at a high temperature. As shown in Supporting Information Figure S4, the glass side will form porous structures after high temperature NR growth, and the transparency of the glass will reduce considerably as shown in

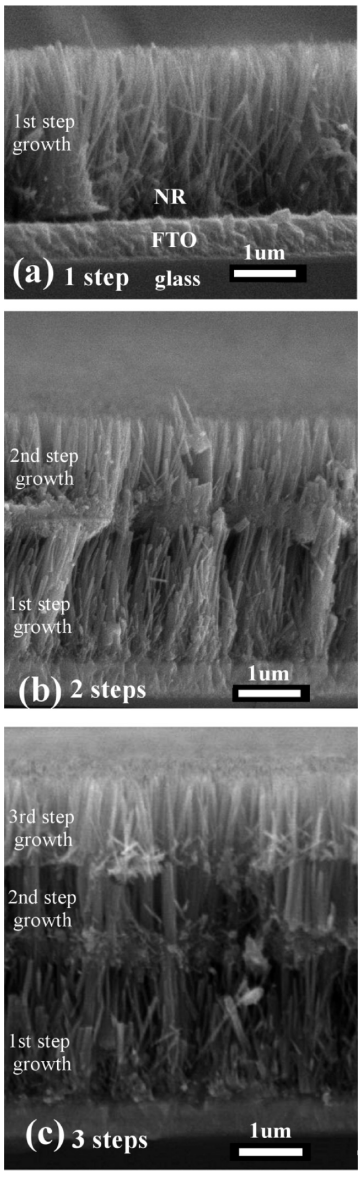

Figure 5. SEM cross-section view of (a) the one-step grown sample (1S), (b) the two-step grown sample (2S), and (c) the three-step grown sample (3S).

Figure S4b. The glass corrosion could be avoidable by using procedures, such as coating the glass side with a protection film, using mixed acid to reduce the harsh reaction condition, and lowering the reaction temperature.

Three NR samples with different growth cycles have been used to assemble DSSC devices to evaluate their performance. The $J-V$ curve and related device performance parameters (fill factor (FF), short circuit current (J_{sc}), and open circuit voltage (V_{oc})) with respect to the NR height are presented in Figure 6. The short circuit current has been increased from 2.7 mA/cm^2 for a device fabricated using sample 1S to 4.5 mA/cm^2 for a device fabricated using sample 2S and 5.3 mA/cm^2 for a device fabricated using sample 3S. The current increase from 2S to 3S is smaller than that from 1S to 2S, which can be attributed to the considerable decrease of the transparency (~30%) of the glass substrate due to the corrosion as shown in Supporting Information Figure S4. The pores formed during long time reaction will scatter the incoming light. The dotted line in Figure 6a reflects the efficiency with a light loss correction. The open circuit voltage is very similar (around 0.67 V) for the three devices. Figure 6b presents the current density, open circuit voltage, and fill factor (FF) as functions of the height of the NR array. The fill factors (FFs) are 0.45, 0.53, and 0.55 for devices fabricated using 1S, 2S, and 3S samples indicating that the FF increases with the increase of the length of the NRs. These stable open circuit voltage and improved FF indicate that the multiple step grown NRs are beneficial to the carrier transport; in other words, the electrons are efficiently transported with a reduced recombination loss.[36] EIS of 1S and 2S NRs based device have been measured as shown in Figure 6c and d. From the Bode plot, the peak position has shifted from 34.9 Hz (1S) to 11.2 Hz (2S), and this lower frequency shift indicates a prolonged lifetime.[15] The enhanced lifetime after MSG implies the good quality of MSG and very limited defects in NRs synthesized by MSG. Furthermore, additional hydrothermal cycle could improve the crystallinity of the NRs and bonding between the NRs and the substrate as indicated by the reduction of the series resistance shown in Figure 6c. In short, our results show that the NRs synthesized from the MSG have improved the performance of the solar cells in both surface area and charge transport aspects.

To have a better understanding of the interface area for the different NR samples, a dye desorption measurement has been carried out and the results are shown in Figure 7. All absorption peaks of the dye N719 increase as the number of growth cycle increases. The dominant peak of fully deprotonated dye is located around 313 nm, which has the extinction coefficient of 4.59×10^4 M^{-1} cm^{-1}.[37] With the 1 nm^2 assumption of the surface area occupied by a single dye molecule, the total effective internal area and roughness factor (RF) can be derived. The RFs for 1S, 2S, and 3S NRs are 153, 272, and 402, respectively. The stable increase of the RFs of the NRs is consistent with the increase of the length of the NRs after multiple step growth. The RF value of our 3S sample is comparable to the reported values.[17,20] Solar cells fabricated using the rutile NR arrays grown from the multiple step with the SAM assistance have the potential to achieve a high energy conversion efficiency if the glass corrosion issue is solved. It should also be mentioned that if the NRs are post-treated such as introducing hierarchical structure,[4,7] the RF may be enhanced further since NRs is relatively sparse from the top view (Supporting Information Figure S3).

The MSG with SAM assistance is a versatile approach for hydrothermally synthesizing the rutile NRs. In order to demonstrate its extensibility, the MSG has been applied to the NRs grown at low temperature (150 °C) followed by acid etching method.[17] Those NRs were denoted as TCE nS (growth using $TiCl_4$ as precursor with a subsequent acid etching, n means the nth step growth.). Since the reaction takes place at a low temperature, the back side of the FTO glass is less affected during several growth cycles. Figure 8 shows the $J-V$ curve of the MSG grown samples after acid etching. The short circuit currents increase from 3.3 mA/cm^2 (for TCE 1S sample) to 6.9 mA/cm^2 (for TCE 2S sample) and 10.3 mA/cm^2 (for TCE 3S sample). The average length of the TCE 3S NRs is 11 μm as shown in the inset in Figure 8. The efficiency of the DSSC made using the TCE 3S NRs reaches to 4.6% a significant increase from 1.2% for DSSC made using the TCE 1S sample, and the FF of the DSSC made of the TCE 3S NRs increases up to 0.68 from 0.54 of the DSSC made of TEC 1S NRs. This beneficial effect comes from several factors. First of

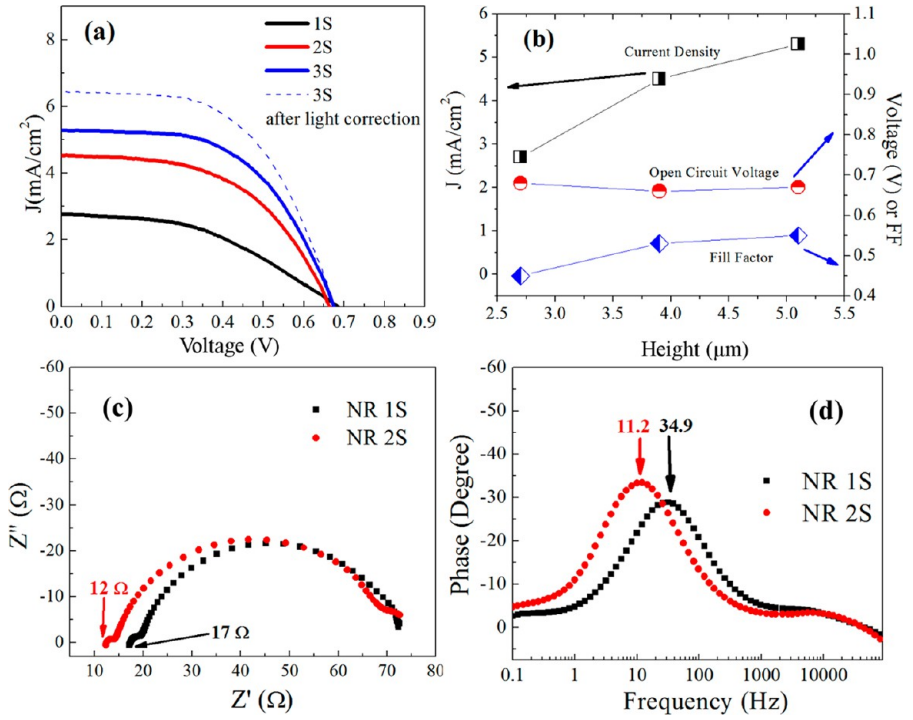

Figure 6. (a) J–V curve of the DSSCs made from the 1S, 2S, and 3S NR sample. (b) The fill factor (FF), short circuit current (J_{sc}), and open circuit voltage (V_{oc}) as a function of the NR height. Electrochemical impedance spectroscopy (EIS) of 1S and 2S NR based devices: Nyquist plot (c) and Bode plot (d).

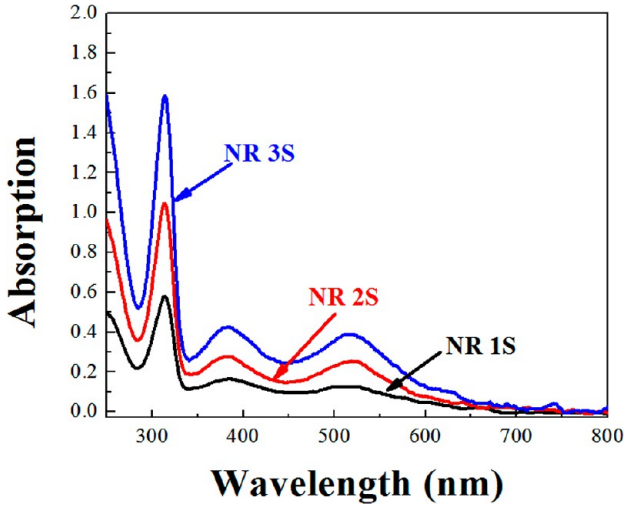

Figure 7. UV–vis absorption spectrum of the dyes absorbed on the 1S, 2S, and 3S NRs sample.

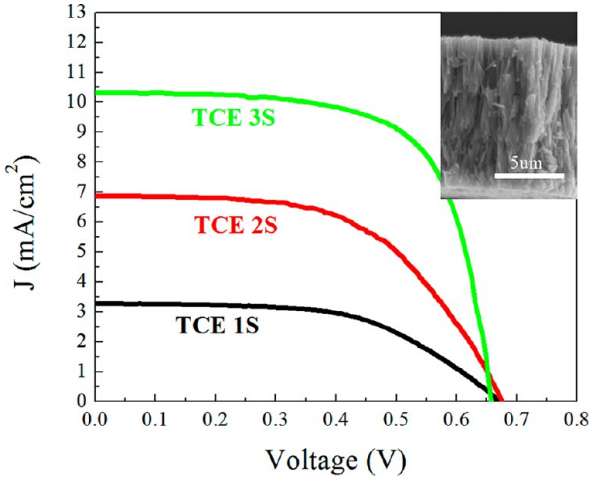

Figure 8. J–V curves from the DSSC devices made of the NRs synthesized with the combination of MSG and the acid etching. The TCE 1S, TCE 2S, and TCE 3S represent the solar cells made using the one-step, two-step, and three-step grown and acid etched NR samples, respectively. (inset) SEM cross-sectional view of the TCE 3S NRs after etching.

all, with the protection of the SAM layer, the porosity of the prior NR array is maintained and the adhesion of the first layer NRs to the FTO substrate is still strong due to the avoidance of the acid etching. The SAM protection prevents the peel-off of the NR array from the FTO glass, which is usually a major challenge in the etching process. Second, the second and the third layer of the NR array have a higher density than that of the first layer NR array as shown in Supporting Information Figure S5. The acid etching will separate the NRs in the bundles resulting in high internal surface area which will enhance the solar cell performance.

CONCLUSION

A versatile multiple step growth of rutile NR with the assistance of ODP SAM has been successfully developed to synthesize rutile NR arrays. The ODP SAM layer is strong enough to endure harsh hydrothermal reaction environment and retains its original hydrophobicity. The anisotropic photocatalysis of the rutile NRs is employed to selectively remove the SAM layer on the tip of the NRs while the SAM layer coated on the side walls of the NRs will remain intact. By applying middle layer of

TiO_2 nanoparticles, NRs with subhundred nanometer width have been grown in multiple cycles, and the NRs grown from different steps have similar width. Devices made from multiple-step grown NRs show a considerable enhancement in their efficiency especially for the NRs grown at low temperature with acid etching. Although the efficiency of the solar cells built using the multiple-step grown NRs is not competitive to NPs at this moment, the MSG method provides an opportunity to boost its current efficiency and is compatible to most hydrothermal reaction approach. It could be combined with the single step growth,[17,38,39] surface treatment and hierarchical structure,[4,7,9] and new types of sensitizer with a high extinction coefficient[40,41] to achieve higher efficiency.

■ ASSOCIATED CONTENT

Supporting Information

Nanorod synthesis procedure, evolution of contact angle over solar light exposure time for SAM treated nanorods sample, cyclic voltammetry measurement of ODP modified NRs, SEM top views of multiple step grown nanorods, and SEM micrograph of glass slide corrosion and related transmission spectrum. This material is available free of charge via the Internet at http://pubs.acs.org

■ AUTHOR INFORMATION

Corresponding Author

*E-mail: wenzhi.li@fiu.edu.

Notes

The authors declare no competing financial interest.

■ ACKNOWLEDGMENTS

W.L. acknowledges the support by The American Chemical Society Petroleum Research Fund under grant no. 51766-ND10. N.P. acknowledges the support by the NSF CAREER program with the Award Number: 1149059 (Program manager: Samir El-Ghazaly).

■ REFERENCES

(1) Law, M.; Greene, L. E.; Johnson, J. C.; Saykally, R.; Yang, P. D. *Nat. Mater.* **2005**, *4*, 455−459.
(2) Xu, C. K.; Shin, P.; Cao, L. L.; Gao, D. *J. Phys. Chem. C* **2010**, *114*, 125−129.
(3) Mor, G. K.; Shankar, K.; Paulose, M.; Varghese, O. K.; Grimes, C. A. *Nano Lett.* **2006**, *6*, 215−218.
(4) Ye, M. D.; Xin, X. K.; Lin, C. J.; Lin, Z. Q. *Nano Lett.* **2011**, *11*, 3214−3220.
(5) Liu, B.; Aydil, E. S. *J. Am. Chem. Soc.* **2009**, *131*, 3985−3990.
(6) Feng, X. J.; Shankar, K.; Varghese, O. K.; Paulose, M.; Latempa, T. J.; Grimes, C. A. *Nano Lett.* **2008**, *8*, 3781−3786.
(7) Liao, J. Y.; Lei, B. X.; Chen, H. Y.; Kuang, D. B.; Su, C. Y. *Energy Environ. Sci.* **2012**, *5*, 5750−5757.
(8) Gubbala, S.; Chakrapani, V.; Kumar, V.; Sunkara, M. K. *Adv. Funct. Mater.* **2008**, *18*, 2411−2418.
(9) Yang, M. J.; Ding, B.; Lee, S.; Lee, J. K. *J. Phys. Chem. C* **2011**, *115*, 14534−14541.
(10) Feng, X.; Zhu, K.; Frank, A. J.; Grimes, C. A.; Mallouk, T. E. *Angew. Chem., Int. Ed.* **2012**, *51*, 2727−2730.
(11) Kim, H.-S.; Lee, J.-W.; Yantara, N.; Boix, P. P.; Kulkarni, S. A.; Mhaisalkar, S.; Grätzel, M.; Park, N.-G. *Nano Lett.* **2013**, *13*, 2412−2417.
(12) Wang, H.; Bai, Y. S.; Wu, Q. O.; Zhou, W.; Zhang, H.; Li, J. H.; Guo, L. *Phys. Chem. Chem. Phys.* **2011**, *13*, 6977−6982.
(13) Cho, I. S.; Chen, Z. B.; Forman, A. J.; Kim, D. R.; Rao, P. M.; Jaramillo, T. F.; Zheng, X. L. *Nano Lett.* **2011**, *11*, 4978−4984.
(14) Zhou, Z. J.; Fan, J. Q.; Wang, X.; Zhou, W. H.; Du, Z. L.; Wu, S. X. *ACS Appl. Mater. Interfaces* **2011**, *3*, 4349−4353.
(15) Wang, X. Y.; Liu, Y.; Zhou, X.; Li, B. J.; Wang, H.; Zhao, W. X.; Huang, H.; Liang, C. L.; Yu, X.; Liu, Z.; Shen, H. *J. Mater. Chem.* **2012**, *22*, 17531−17538.
(16) Guo, W. X.; Xu, C.; Wang, X.; Wang, S. H.; Pan, C. F.; Lin, C. J.; Wang, Z. L. *J. Am. Chem. Soc.* **2012**, *134*, 4437−4441.
(17) Lv, M. Q.; Zheng, D. J.; Ye, M. D.; Sun, L.; Xiao, J.; Guo, W. X.; Lin, C. J. *Nanoscale* **2012**, *4*, 5872−5879.
(18) Lv, M. Q.; Zheng, D. J.; Ye, M. D.; Xiao, J.; Guo, W. X.; Lai, Y. K.; Sun, L.; Lin, C. J.; Zuo, J. *Energy Environ. Sci.* **2013**, *6*, 1615−1622.
(19) Wu, W. Q.; Lei, B. X.; Rao, H. S.; Xu, Y. F.; Wang, Y. F.; Su, C. Y.; Kuang, D. B. *Sci. Rep.* **2013**, *3*, No. 1352, DOI: 10.1038/srep01352.
(20) Xu, C. K.; Wu, J. M.; Desai, U. V.; Gao, D. *J. Am. Chem. Soc.* **2011**, *133*, 8122−8125.
(21) Marcinko, S.; Fadeev, A. Y. *Langmuir* **2004**, *20*, 2270−2273.
(22) Helmy, R.; Fadeev, A. Y. *Langmuir* **2002**, *18*, 8924−8928.
(23) Zhang, X. T.; Jin, M.; Liu, Z. Y.; Nishimoto, S.; Saito, H.; Murakami, T.; Fujishima, A. *Langmuir* **2006**, *22*, 9477−9479.
(24) Balaur, E.; Macak, J. M.; Taveira, L.; Schmuki, P. *Electrochem. Commun.* **2005**, *7*, 1066−1070.
(25) Liu, G.; Yu, J. C.; Lu, G. Q.; Cheng, H. M. *Chem. Commun.* **2011**, *47*, 6763−6783.
(26) Dessombz, A.; Chiche, D.; Davidson, P.; Panine, P.; Chaneac, C.; Jolivet, J. P. *J. Am. Chem. Soc.* **2007**, *129*, 5904−5909.
(27) Ahmed, A. Y.; Kandiel, T. A.; Oekermann, T.; Bahnemann, D. *J. Phys. Chem. Lett.* **2011**, *2*, 2461−2465.
(28) Zhang, X. T.; Jin, M.; Liu, Z. Y.; Tryk, D. A.; Nishimoto, S.; Murakami, T.; Fujishima, A. *J. Phys. Chem. C* **2007**, *111*, 14521−14529.
(29) Neale, N. R.; Kopidakis, N.; van de Lagemaat, J.; Gratzel, M.; Frank, A. J. *J. Phys. Chem. B* **2005**, *109*, 23183−23189.
(30) Parker, A. R.; Lawrence, C. R. *Nature* **2001**, *414*, 33−34.
(31) Wang, R.; Hashimoto, K.; Fujishima, A.; Chikuni, M.; Kojima, E.; Kitamura, A.; Shimohigoshi, M.; Watanabe, T. *Nature* **1997**, *388*, 431−432.
(32) Wang, R.; Sakai, N.; Fujishima, A.; Watanabe, T.; Hashimoto, K. *J. Phys. Chem. B* **1999**, *103*, 2188−2194.
(33) Feng, X. J.; Zhai, J.; Jiang, L. *Angew. Chem., Int. Ed.* **2005**, *44*, 5115−5118.
(34) Miyauchi, M.; Kieda, N.; Hishita, S.; Mitsuhashi, T.; Nakajima, A.; Watanabe, T.; Hashimoto, K. *Surf. Sci.* **2002**, *511*, 401−407.
(35) Baxter, J. B.; Walker, A. M.; van Ommering, K.; Aydil, E. S. *Nanotechnology* **2006**, *17*, S304−S312.
(36) Tan, B.; Wu, Y. Y. *J. Phys. Chem. B* **2006**, *110*, 15932−15938.
(37) Nazeeruddin, M. K.; Zakeeruddin, S. M.; Humphry-Baker, R.; Jirousek, M.; Liska, P.; Vlachopoulos, N.; Shklover, V.; Fischer, C. H.; Gratzel, M. *Inorg. Chem.* **1999**, *38*, 6298−6305.
(38) Huang, Q. L.; Zhou, G.; Fang, L.; Hu, L. P.; Wang, Z. S. *Energy Environ. Sci.* **2011**, *4*, 2145−2151.
(39) Yang, M. J.; Ding, B.; Lee, J.-K. *J. Power Sources* **2014**, *245*, 301−307.
(40) Lee, J. K.; Yang, M. J. *Mater. Sci. Eng., B* **2011**, *176*, 1142−1160.
(41) Miyasaka, T. *J. Phys. Chem. Lett.* **2011**, *2*, 262−269.